Hindawi Publishing Corporation
Journal of Nanomaterials
Volume 2014, Article ID 498131, 8 pages
http://dx.doi.org/10.1155/2014/498131

Research Article

Fabrication of Aligned Carbon Nanotube/Polycaprolactone/Gelatin Nanofibrous Matrices for Schwann Cell Immobilization

Shiao-Wen Tsai,[1] Chun-Chiang Huang,[2] Lih-Rou Rau,[1] and Fu-Yin Hsu[2,3]

[1] *Graduate Institute of Biochemical and Biomedical Engineering, Chang-Gung University, Taoyuan 33333, Taiwan*
[2] *Institute of Bioscience and Biotechnology, National Taiwan Ocean University, Keelung 20224, Taiwan*
[3] *Department of Life Sciences, National Taiwan Ocean University, Keelung 20224, Taiwan*

Correspondence should be addressed to Fu-Yin Hsu; fyhsu5565@gmail.com

Received 10 February 2014; Accepted 27 March 2014; Published 14 May 2014

Academic Editor: Ruigang Liu

In this study, we utilized a mandrel rotating collector consisting of two parallel, electrically conductive pieces of tape to fabricate aligned electrospun polycaprolactone/gelatin (PG) and carbon nanotube/polycaprolactone/gelatin (PGC) nanofibrous matrices. Furthermore, we examined the biological performance of the PGC nanofibrous and film matrices using an *in vitro* culture of RT4-D6P2T rat Schwann cells. Using cell adhesion tests, we found that carbon nanotube inhibited Schwann cell attachment on PGC nanofibrous and film matrices. However, the proliferation rates of Schwann cells were higher when they were immobilized on PGC nanofibrous matrices compared to PGC film matrices. Using western blot analysis, we found that NRG1 and P0 protein expression levels were higher for cells immobilized on PGC nanofibrous matrices compared to PG nanofibrous matrices. However, the carbon nanotube inhibited NRG1 and P0 protein expression in cells immobilized on PGC film matrices. Moreover, the NRG1 and P0 protein expression levels were higher for cells immobilized on PGC nanofibrous matrices compared to PGC film matrices. We found that the matrix topography and composition influenced Schwann cell behavior.

1. Introduction

Nerve autografts are considered the "gold standard" for the repair of long gaps caused by nerve damage. These materials are harvested from another site in the body and are typically not rejected by the immune system. Nevertheless, the harvesting step requires an additional surgical procedure that can cause donor site morbidity and patient discomfort. Allografts, obtained from human cadavers or living donors, often are rejected by the host; thus, their efficiency, application, and availability are limited [1–3]. Nerve grafts made of natural and synthetic materials are thus a promising alternative for promoting successful nerve regeneration because they have the potential to overcome many of the drawbacks associated with autologous and allogeneic nerve grafting.

Polycaprolactone (PCL) has recently been used in a variety of tissue engineering applications because of its high toughness and cost efficiency [4]. However, cells exposed to PCL do not behave favorably because PCL has lower hydrophilicity than natural ECM. Gelatin is obtained by partial hydrolysis of native collagen in acidic or alkaline environments. Gelatin exhibits excellent biocompatibility and biodegradability, and it has been widely used as a component in many biomedical materials, including wound dressings, drug release structures, and tissue-engineered bone, skin, cartilage, and nerve [5, 6]. Carbon nanotubes (CNTs) are promising for use in regenerative medicine due to their unique electrical, mechanical, chemical, and biological properties and their ease of combination with various biological compounds [7, 8]. When CNTs are incorporated into biopolymers, electrically conductive scaffolds that can support both Schwann cells and neurons can be synthesized [9].

Electrospinning can be readily utilized to fabricate ultrafine fibers with average diameters ranging from the submicrometer to nanometer scale. Advantageously, fibrous

matrices that have been synthesized using electrospinning display high specific surface areas, high aspect ratios, and high porosity surfaces. More importantly, the topological structures of these matrices can mimic that of the extracellular matrix and enhance cell migration, proliferation, and differentiation [10, 11].

Aligned fibers prepared via electrospinning enhance Schwann cell maturation to a greater degree compared to randomly oriented fibers [12]. In the past, aligned fibers have been produced using a variety of methods [13, 14]. Li et al. fabricated aligned nanofibers using a collector consisting of two parallel, electrically conductive substrates separated by a gap [15]. Matthews et al. collected circumferentially aligned electrospun fibers on a mandrel rotating at a high speed [16]. In this paper, we discuss the fabrication of electrospun nanofibrous matrices in which the fibers are aligned along the longitudinal axis of a mandrel using a rotating collector containing two parallel, electrically conductive pieces of tape.

It is challenging and difficult to promote nervous system regeneration. However, the peripheral nervous system has an intrinsic ability to repair and regenerate axons; Schwann cells enhance such regeneration after damage occurs [17]. The aim of this study was to fabricate aligned carbon nanotube/polycaprolactone/gelatin nanofibrous matrices and investigate their potential as neurografts for peripheral nerve repair.

2. Materials and Methods

2.1. Reagents. Gelatin (type A) and polycaprolactone were purchased from the Sigma Aldrich Chemical Company (St. Louis, MO, USA). Carbon nanotubes were purchased from the Golden Innovation Business Co. Ltd. (New Taipei City, Taiwan). RT4-D6P2T rat Schwann cells were purchased from the BCRC (Bioresource Collection and Research Center, Hsinchu, Taiwan). Dulbecco's modified Eagle medium (DMEM), fetal bovine serum (FBS), and trypsin were purchased from GIBCO (Grand Island, NY, USA). All of the other chemicals used herein were of reagent grade unless stated otherwise.

2.2. Acid-Oxidized CNTs. The surfaces of the CNTs were functionalized according to the method delineated by Xiao et al. [18]. Briefly, 0.1 g of pristine CNTs was added to 20 mL of hydrochloric acid (36.5 wt%) and stirred for 2 hours at a moderate speed. Then, the CNTs were diluted with water, filtered, washed with deionized water, and dried under vacuum at 60°C overnight. Afterward, the pretreated CNTs were put into 15 mL of nitric acid (HNO_3) (65 wt%) and heated at 140°C for 4 hours. The CNTs were subsequently cooled to room temperature; then the entire of acid-oxidized CNT process was repeated one time.

2.3. Characterization of Acid-Oxidized CNTs. ATR-FTIR spectra of pristine and acid-oxidized CNTs were obtained using a Bruker spectrometer. The spectra were obtained using 64 scans with a resolution of 4 cm^{-1} in the range of 600–4000 cm^{-1}.

2.4. Preparation of CNT/Polycaprolactone/Gelatin Nanofibrous Matrices. Gelatin and polycaprolactone powders (42.5 mg of each) were dissolved in 1 mL 1,1,1,3,3,3-hexafluoro-2-propanol (HFIP). Acid-oxidized CNTs were then added to the HFIP solution of polycaprolactone/gelatin and dissolved using vortexing until the solution became homogeneous. In preparation for electrospinning, the polymer solution was placed into a 5 mL syringe fitted with a needle (tip diameter = 0.96 mm) and attached to a syringe pump that provided a steady solution flow rate. A voltage was applied to the needle using a high voltage power supply; the tip-to-collector distance was fixed.

2.5. Preparation of CNT/Polycaprolactone/Gelatin Films. CNT/polycaprolactone/gelatin (PGC) thin films were prepared using the spin-coating method. The PGC solution was spin-coated onto cover glass (diameter = 10 mm) at 4000 rpm for 3 seconds. The films were dried in air at room temperature.

2.6. Characterization of the Electrospun Nanofibers. The morphologies of the PG and PGC fibers were examined by scanning electron microscopy (Hitachi S-4800). Briefly, the electrospun matrices were sputter-coated with gold and then visualized using a scanning electron microscope (accelerating voltage = 5 kV). The diameters of the fibers were determined manually from the SEM images using ImageJ (ImageJ software 1.42, National Institutes of Health, USA).

2.7. Schwann Cell Culture on PG and PGC Matrices. PG and PGC matrices were placed in 24-well tissue culture plates containing a suspension of RT4-D6P2T rat Schwann cells (BCRC no. 60508) (5×10^4 cells/well) in DMEM supplemented with 10% v/v FBS, 100 U/mL of penicillin, and 100 μg/mL of streptomycin. The cultures of these cell-seeded matrices were harvested after 4 hours so that cell attachment assays could be completed and on days 1, 3, 5, and 7 so that cell proliferation assays could be performed. Cell viabilities were determined using MTT assays. In each experiment, the amount of dye formed was immediately measured using a microplate reader (Biotek uQuant) (wavelength = 570 nm). At each time point, the number of cells attached to three matrices was measured.

2.8. Fluorescent Staining of the Cytoskeleton. The morphologies of the cells were examined by fluorescently staining their F-actin cytoskeletons with fluorescein isothiocyanate-(FITC-) conjugated phalloidin and their nuclei with DAPI. Cells were cultured for 1 day, fixed with 3.7% paraformaldehyde in phosphate buffer for 10 minutes, and washed twice with 0.02 M PBS (pH 7.4). The cells were then rinsed in PBS containing 0.1% Triton X-100 for 5 minutes. The samples were blocked with 1% bovine serum albumin (BSA) in PBS for 1 hour to reduce nonspecific background staining. After blocking, the BSA solution was aspirated, and the samples were incubated with 6.4 μM FITC-conjugated phalloidin for 20 minutes. The cells were then incubated with a solution of DAPI for 5 minutes to stain the DNA in the cells. The samples

Table 1: Sample notation, electrospinning parameters, and average diameters of random PG and PGC nanofibers.

Sample notation	Polycaprolactone concentration (mg/mL)	Gelatin concentration (mg/mL)	Carbon nanotube concentration (mg/mL)	Electrospinning parameters (applied voltage, working distance, and flow rate)	Average diameter ± standard deviation (nm)
PG	42.55	42.55	0	15 kV, 15 cm, 3.81 mL/hour	671 ± 145
PG3C	42.55	42.55	3.54	15 kV, 15 cm, 3.81 mL/hour	331 ± 111
PG5C	42.55	42.55	4.47	15 kV, 15 cm, 3.81 mL/hour	440 ± 140

were washed three times with PBS (for 5 minutes each) and analyzed using a fluorescence microscope.

2.9. Immunoblotting Analysis. Cells were seeded on PG and PGC matrices (3×10^4 cells/cm^2, in media). Immunoblotting was performed to detect the Schwann cell-specific proteins neuregulin 1 (NRG1) and myelin protein zero (P0) after 3 days of culture. Cells were collected and lysed in lysis buffer. The supernatants were obtained by centrifugation (15,000 ×g for 10 minutes) at 4°C. The concentration of protein was analyzed using a Bradford Coomassie assay. The proteins (30 μg/μL) were fractionated by electrophoresis and electrotransferred to a polyvinylidene difluoride film (PVDF). Blocking was performed using 5% w/v nonfat milk, and primary antibodies were applied to the membrane overnight at 4°C. The primary antibodies were diluted with fresh blocking buffer to the designated concentration and applied to the membrane at 4°C overnight. Antibodies specific to NRG1 (Santa Cruz Biotechnology, Inc., sc-28916), P0 (Santa Cruz Biotechnology, Inc., sc-18531), and nucleophosmin B23 (Invitrogen 325200) were used. After incubation with a secondary antibody, the immunoreactive bands were visualized using enhanced chemiluminescence detection (Millipore WBKLS0500). Nucleophosmin B23 was used as the internal control.

3. Results and Discussion

The pristine CNTs were quite hydrophobic. Hence, the pristine CNTs precipitated from the HFIP solution. Nitric acid was used to introduce oxygen-containing functional groups, such as carboxylic acids and hydroxyls, onto the ends and defect sites of the CNT surfaces [19]. Figure 1 shows the ATR-FTIR spectra of pristine CNTs and acid-oxidized CNTs. The absorption peaks centered at 1594 cm^{-1} correspond to the asymmetric –COO– stretching bands. The absorption peaks at 3443 cm^{-1} correspond to the –OH stretch. We found that the acid-oxidized CNTs have better dispersibility in HFIP. The zeta potentials of the pristine CNTs and acid-oxidized CNTs were measured to be −5.05 ± 0.56 mV and −23.8 ± 0.87 mV, respectively.

Figure 2 shows transmission electron microscopy images of nanofibers containing PG and PGC. Individual CNTs were successfully embedded in the polycaprolactone/gelatin nanofibers, indicating that the original dispersion contained individual CNTs rather than CNT aggregates.

Under the same electrospinning conditions, the fiber diameters were 671 ± 145 nm, 331 ± 111 nm, and 440 ± 140 nm

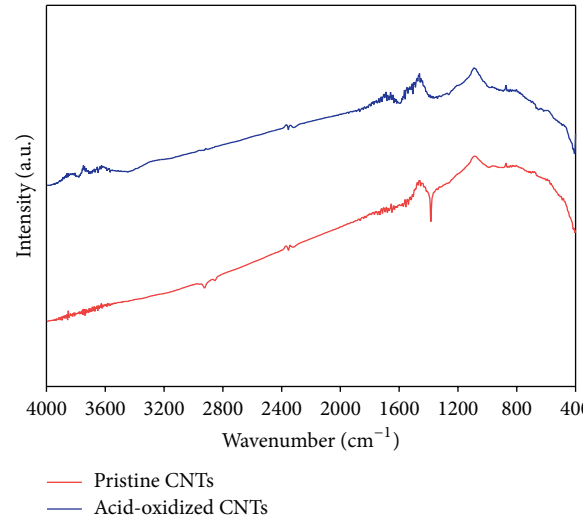

Figure 1: ATR-FTIR spectra of pristine CNTs and acid-oxidized CNTs.

for PG, PG3C, and PG5C matrices, respectively (Table 1 and Figure 3). The diameters of the fibers decreased and then increased as the concentration of CNTs was increased. The conductivity of the polymer was increased when the CNTs were added. Previously, we found that when the charge density on the surface of the electrospinning jet was increased, higher electrostatic forces were induced, resulting in the formation of smaller diameter fibers [20]. In addition, the viscosity of the polymer solution also affects the diameter of the nanofibers. The diameters of the electrospun fibers increased as the viscosity of the polymer solution increased [21]. The viscosity of the polymer solution also increased when CNTs were added. These factors likely explain why the mean fiber diameters decrease when lower CNTs concentrations are used and increase when higher CNTs concentrations are used.

A schematic of the experimental setup used to align the fibers is shown in Figure 4(a). A cylinder collector was used to gather the aligned nanofibers. The radius of the cylinder collector was 7.6 cm, and the rotation speed of the mandrel was set to 13 rpm. The distance between the two pieces of parallel conductive carbon tape was 2 cm. A cross section of the cylinder collector is shown in Figure 4(b). The literature has demonstrated that the diameters of the electrospun fibers can affect cell behavior [22–24]. We fabricated aligned PG and aligned PGC fibers with similar diameters by adjusting the parameters of the experiment.

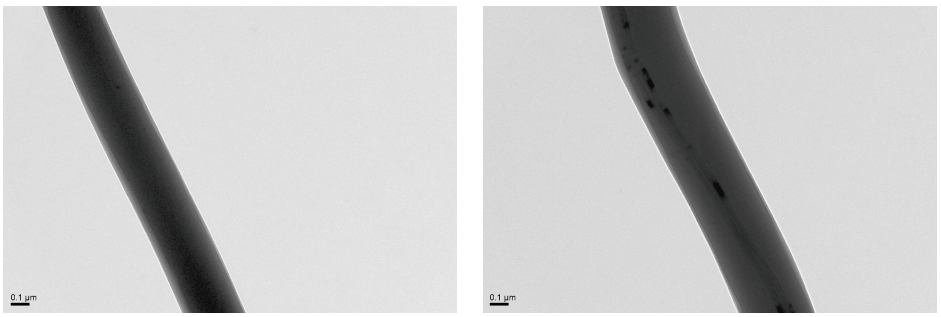

(a) (b)

Figure 2: Transmission electron microscopy images of (a) a PG and (b) a PGC nanofiber.

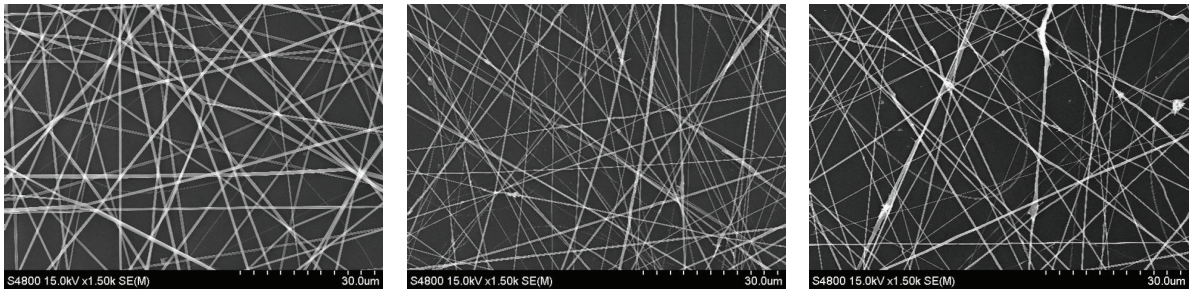

(a) (b) (c)

Figure 3: Scanning electron microscopy images of randomly oriented (a) PG, (b) PG3C, and (c) PG5C nanofibers.

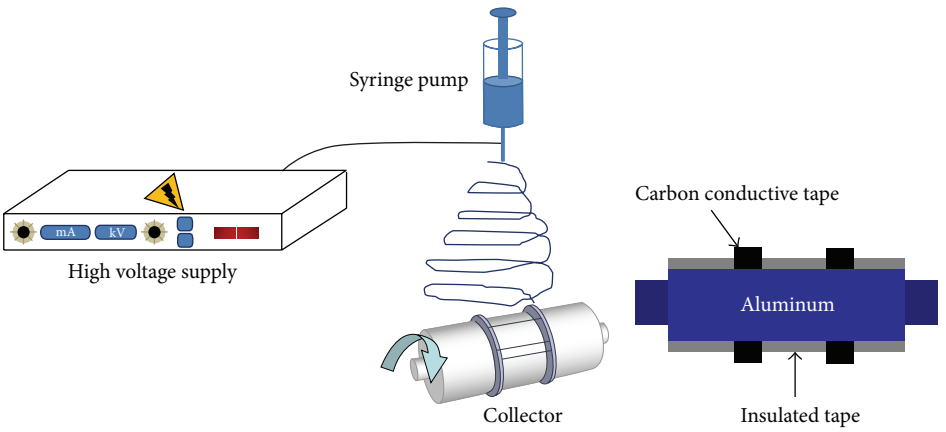

(a) (b)

Figure 4: (a) Schematic illustration of the electrospinning setup. (b) Profile of the aligned nanofiber collector.

Table 2: Sample notation, electrospinning parameters, average diameters, and angular distributions of aligned PG and PGC nanofibers.

Sample notation	Polycaprolactone concentration (mg/mL)	Gelatin concentration (mg/mL)	Carbon nanotube concentration (mg/mL)	Electrospinning parameters (applied voltage, working distance, and flow rate)	Average diameter ± standard deviation (nm)	Angular distribution of aligned nanofibers (full width at half maximum, degrees)
PG	42.55	42.55	0	15 kV, 15 cm, 0.51 mL/hour	785 ± 155	26
PG3C	42.55	42.55	3.54	20 kV, 15 cm, 0.76 mL/hour	828 ± 169	21
PG5C	42.55	42.55	4.47	20 kV, 10 cm, 6.36 mL/hour	710 ± 156	43

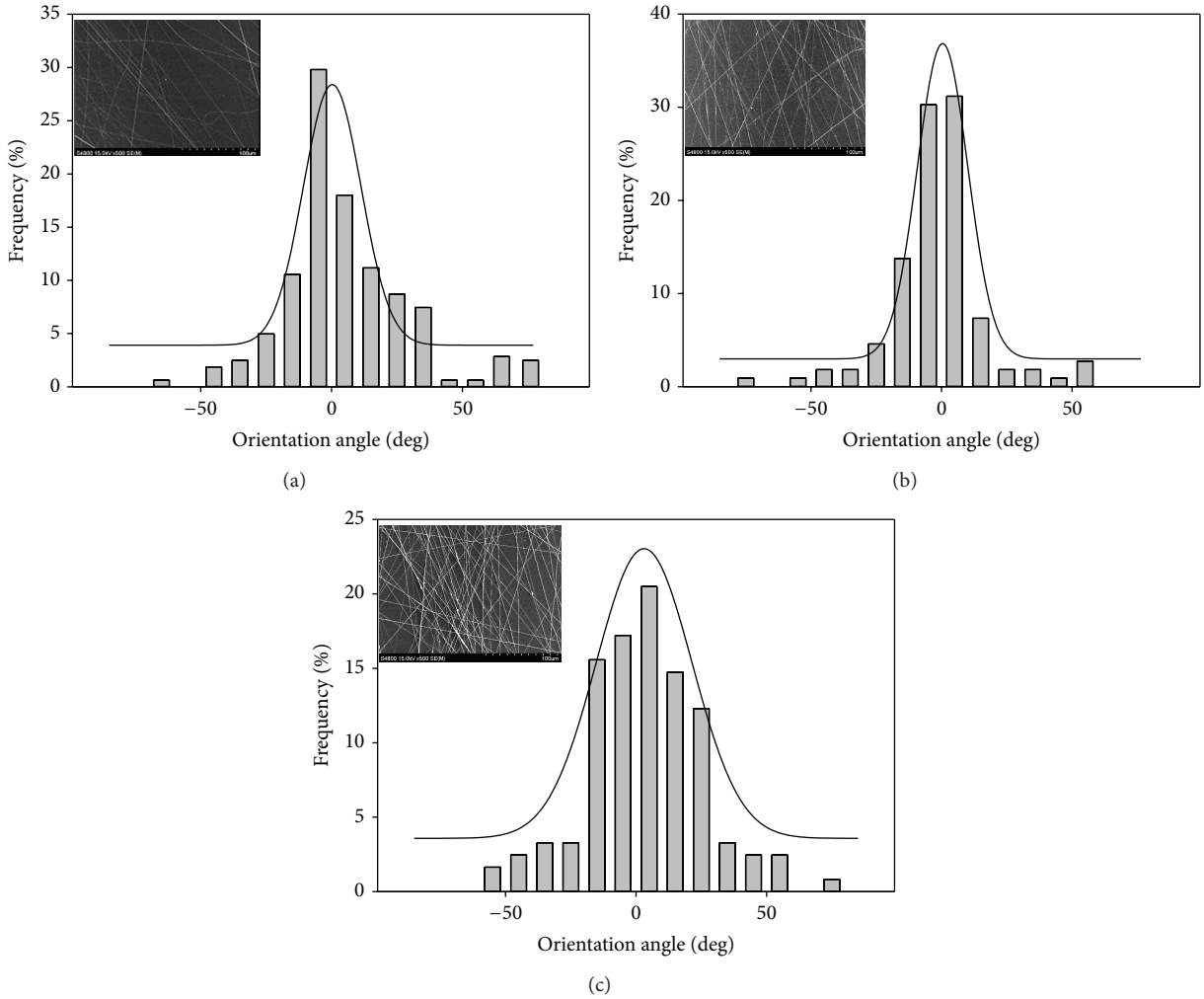

Figure 5: Distributions of the orientation angles between the long axes of the nanofibers and their expected directions: (a) PG, (b) PG3C, and (c) PG5C. The black lines are Gaussian fits to the data. These results were based on measurements of more than 100 nanofibers. The insets show scanning electron microscopy images of the corresponding nanofibers.

The diameters of the synthesized fibers were 785 ± 155 nm, 828 ± 169 nm, and 710 ± 156 nm for the PG, PG3C, and PG5C systems, respectively (Figure 5 and Table 2). The diameters of these fibers were not significantly different ($P > 0.05$). The average orientation angles of the nanofibers were measured using SEM. The angular distributions of the nanofibers were determined by fitting the relative frequencies of the angle between the long axes of the fibers and their expected direction for each sample to a Gaussian curve. The full width at half maximum (FWHM) values of these curves was 26°, 21°, and 43° for the PG, PG3C, and PG5C samples, respectively (Figure 5). In the past, researchers have used high-speed (>500 rpm) rotating cylinder collectors to fabricate aligned electrospun nanofibers [25, 26]. In this study, we fabricated aligned electrospun nanofibrous matrices at much slower speeds; the alignment direction of the nanofibers is along the longitudinal axis of the mandrel. However, we found that the CNTs influenced the alignment of the nanofibers.

Cell behaviors, including adhesion, spreading, proliferation, and differentiation, are sensitive to the surface topography and molecular composition of the matrix. To evaluate the effect of the CNTs on cell behavior, we incubated RT4-D6P2T rat Schwann cells on PG and PGC nanofiber and film matrices. The attachment and proliferation rates of the Schwann cells gradually decreased when the amount of CNTs was gradually increased when either PGC nanofiber matrices or PGC film matrices were used (Figure 6). Behan et al. [9] found that although CNTs have little effect on Schwann cell viability, they do inhibit their ability to proliferate. Kaiser et al. [27, 28] also demonstrated that CNTs can attach to integrin receptors and can therefore affect cell functions, such as adhesion, spreading, focal adhesion, and cytoskeletal development. Schwann cells proliferated more actively on PGC nanofiber matrices than on PGC film matrices. The CNTs likely disperse on the surface of the PGC film matrices and directly interfere with cell proliferation (Figure 7). However, the CNTs are embedded in the nanofibers of

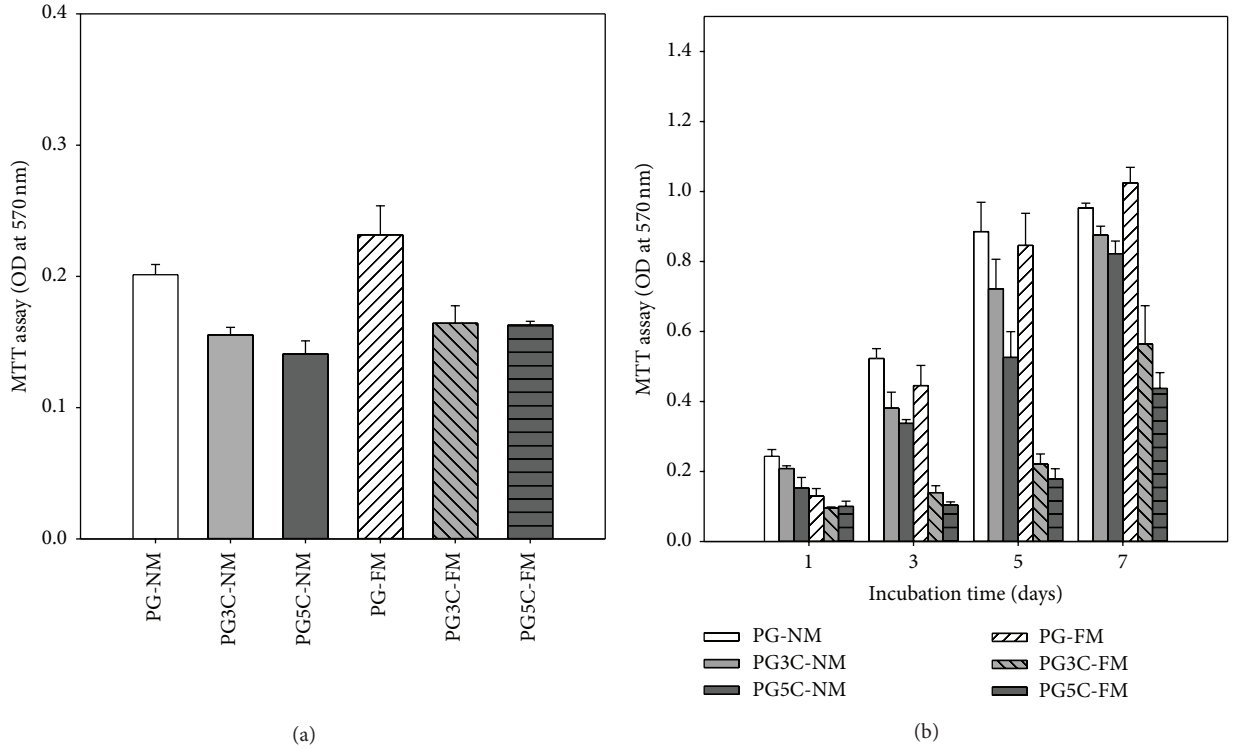

Figure 6: (a) The attachment of RT4-D6P2T Schwann cell lines on various matrices after 4 hours of culturing. (b) The viabilities of RT4-D6P2T Schwann cell lines on various matrices after up to 7 days of culture as assessed by the MTT method. Data are presented as the mean ± SD ($n = 6$).

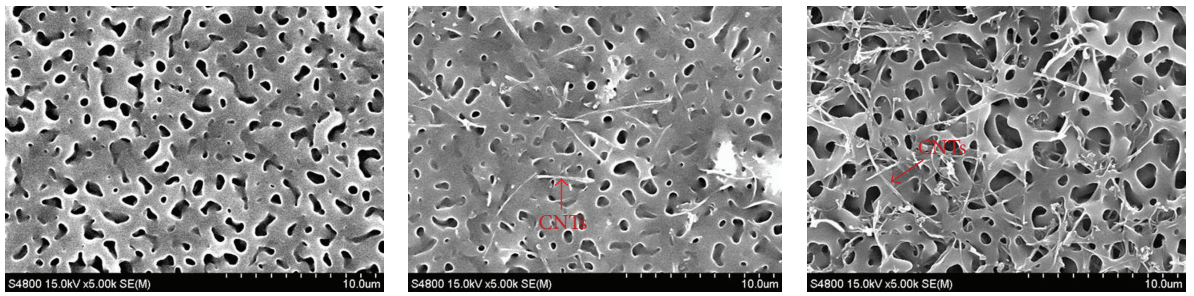

Figure 7: Scanning electron microscopy images of (a) PG, (b) PG3C, and (c) PG5C film matrices.

the PGC nanofibrous matrices, reducing their interaction with the Schwann cells.

The morphologies of the Schwann cells that adhered to the PG and PGC nanofiber and film matrices were investigated. Their actin cytoskeletons were stained with FITC-phalloidin and visualized using a fluorescence microscope. The Schwann cells aligned along the direction of the nanofibers with typical bipolar morphologies (Figures 8(a)–8(c)). However, Schwann cells attached to the film matrices in random directions (Figures 8(d)–8(f)).

Schwann cells are heavily involved in the peripheral nerve repair process. These cells synthesize and secrete important substances, such as myelin protein zero (P0) and neuregulin 1 (NRG1). NRG1 is essential for the myelination of axons and the development of Schwann cells [29]. P0 is expressed by myelinating Schwann cells, and it is the major adhesive and structural protein of the myelin sheath surrounding peripheral nerves [30, 31]. Some studies have demonstrated that P0 promotes the regeneration of injured axons [32]. Using western blot analysis, we found that the NRG1 and P0 protein expression levels were higher for cells immobilized on the PGC nanofibrous matrices than for those immobilized on the PG nanofibrous matrices. However, the CNTs inhibited NRG1 and P0 protein expression in Schwann cells immobilized on the PGC film matrices. Moreover, the NRG1 and P0 protein expression levels were higher for cells immobilized on the PGC nanofibrous matrices than for those immobilized on the PGC film matrices (Figure 9). These results suggest that

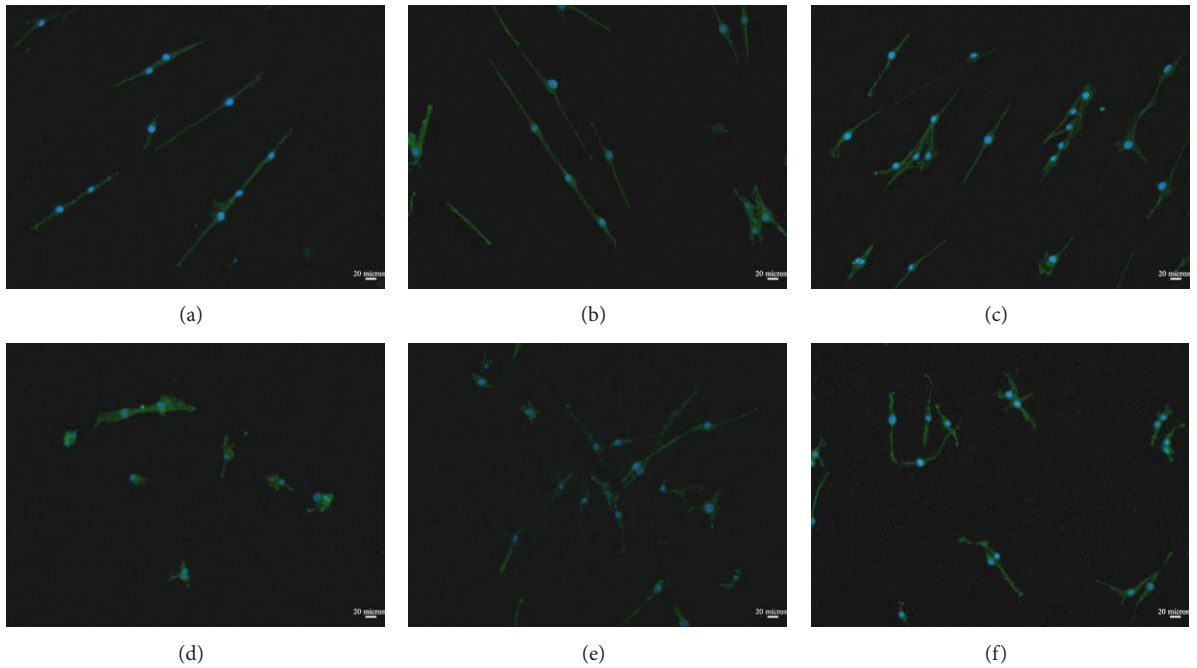

Figure 8: Fluorescent microscopy micrographs of RT4-D6P2T Schwann cell lines cultured for 1 hour on electrospun matrices of (a) PG-NM, (b) PG3C-NM, (c) PG5C-NM, (d) PG-FM, (e) PG3C-FM, and (f) PG5C-FM. NM: nanofibrous matrix; FM: film matrix.

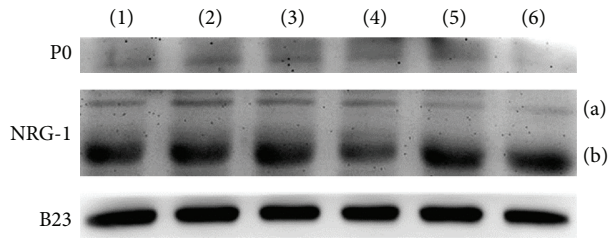

Figure 9: Western blot analyses of NRG1, P0, and B23 proteins in RT4-D6P2T Schwann cells cultured for 3 days. Line 1: PG-NM, Line 2: PG3C-NM, Line 3: PG5C-NM, Line 4: PG-FM, Line 5: PG3C-FM, and Line 6: PG5C-FM. NM: nanofibrous matrix; FM: film matrix. Nrg1: (a) neuregulin 1 precursor and (b) mature neuregulin 1.

Schwann cell maturation is favored on fibrous matrices, as opposed to film matrices, and that CNTs enhance Schwann cell maturation on PGC fibrous matrices.

4. Conclusion

Schwann cells grown on aligned CNT/polycaprolacto-ne/gelatin nanofibrous matrices show higher cell proliferation levels, align along the directionality of the nanofibres with typical bipolar morphologies, and exhibit higher levels of P0 protein expression compared to those grown on CNT/polycaprolactone/gelatin film matrices. These findings suggest that the CNT/polycaprolacto-ne/gelatin nanofibrous matrices could potentially be used for the repair of injured peripheral nerves.

Conflict of Interests

The authors declare that there is no conflict of interests regarding the publication of this paper.

References

[1] T. E. Trumble and F. G. Shon, "The physiology of nerve transplantation," *Hand Clinics*, vol. 16, no. 1, pp. 105–122, 2000.

[2] P. J. Evans, R. Midha, and S. E. Mackinnon, "The peripheral nerve allograft: a comprehensive review of regeneration and neuroimmunology," *Progress in Neurobiology*, vol. 43, no. 3, pp. 187–233, 1994.

[3] J. L. Platt, G. M. Vercellotti, A. P. Dalmasso et al., "Transplantation of discordant xenografts: a review of progress," *Immunology Today*, vol. 11, no. 12, pp. 450–457, 1990.

[4] H. M. Lin, Y. H. Lin, and F. Y. Hsu, "Preparation and characterization of mesoporous bioactive glass/polycaprolactone nanofibrous matrix for bone tissues engineering," *Journal of Materials Science: Materials in Medicine*, vol. 23, no. 11, pp. 2619–2630, 2012.

[5] H. M. Liou, L. R. Rau, C. C. Huang, M. R. Lu, and F. Y. Hsu, "Electrospun hyaluronan-gelatin nanofibrous matrix for nerve tissue engineering," *Journal of Nanomaterials*, vol. 2013, Article ID 613638, 9 pages, 2013.

[6] J. Zhan and P. Lan, "The review on electrospun gelatin fiber scaffold," *Journal of Research Updates in Polymer Science*, vol. 1, no. 2, pp. 59–71, 2012.

[7] F. Mottaghitalab, M. Farokhi, A. Zaminy et al., "A biosynthetic nerve guide conduit based on silk/SWNT/fibronectin nanocomposite for peripheral nerve regeneration," *PLoS ONE*, vol. 8, no. 10, Article ID e74417, 2013.

[8] A. Fabbro, M. Prato, and L. Ballerini, "Carbon nanotubes in neuroregeneration and repair," *Advanced Drug Delivery Reviews*, vol. 65, no. 15, pp. 2034–2044, 2013.

[9] B. L. Behan, D. G. DeWitt, D. R. Bogdanowicz, A. N. Koppes, S. S. Bale, and D. M. Thompson, "Single-walled carbon nanotubes alter Schwann cell behavior differentially within 2D and 3D environments," *Journal of Biomedical Materials Research A*, vol. 96, no. 1, pp. 46–57, 2011.

[10] S. Liao, B. Li, Z. Ma, H. Wei, C. Chan, and S. Ramakrishna, "Biomimetic electrospun nanofibers for tissue regeneration," *Biomedical Materials*, vol. 1, no. 3, pp. R45–R53, 2006.

[11] D. R. Nisbet, J. S. Forsythe, W. Shen, D. I. Finkelstein, and M. K. Horne, "Review paper: a review of the cellular response on electrospun nanofibers for tissue engineering," *Journal of Biomaterials Applications*, vol. 24, no. 1, pp. 7–29, 2009.

[12] S. Y. Chew, R. Mi, A. Hoke, and K. W. Leong, "The effect of the alignment of electrospun fibrous scaffolds on Schwann cell maturation," *Biomaterials*, vol. 29, no. 6, pp. 653–661, 2008.

[13] P. Katta, M. Alessandro, R. D. Ramsier, and G. G. Chase, "Continuous electrospinning of aligned polymer nanofibers onto a wire drum collector," *Nano Letters*, vol. 4, no. 11, pp. 2215–2218, 2004.

[14] W. E. Teo, M. Kotaki, X. M. Mo, and S. Ramakrishna, "Porous tubular structures with controlled fibre orientation using a modified electrospinning method," *Nanotechnology*, vol. 16, no. 6, pp. 918–924, 2005.

[15] D. Li, Y. Wang, and Y. Xia, "Electrospinning of polymeric and ceramic nanofibers as uniaxially aligned arrays," *Nano Letters*, vol. 3, no. 8, pp. 1167–1171, 2003.

[16] J. A. Matthews, G. E. Wnek, D. G. Simpson, and G. L. Bowlin, "Electrospinning of collagen nanofibers," *Biomacromolecules*, vol. 3, no. 2, pp. 232–238, 2002.

[17] T. A. Ferguson and Y. J. Son, "Extrinsic and intrinsic determinants of nerve regeneration," *Journal of Tissue Engineering*, vol. 2, no. 1, Article ID 2041731411418392, 2011.

[18] Y. Xiao, T. Gong, and S. Zhou, "The functionalization of multi-walled carbon nanotubes by in situ deposition of hydroxyapatite," *Biomaterials*, vol. 31, no. 19, pp. 5182–5190, 2010.

[19] V. Datsyuk, M. Kalyva, K. Papagelis et al., "Chemical oxidation of multiwalled carbon nanotubes," *Carbon*, vol. 46, no. 6, pp. 833–840, 2008.

[20] F. Y. Hsu, Y. S. Hung, H. M. Liou, and C. H. Shen, "Electrospun hyaluronate-collagen nanofibrous matrix and the effects of varying the concentration of hyaluronate on the characteristics of foreskin fibroblast cells," *Acta Biomaterialia*, vol. 6, no. 6, pp. 2140–2147, 2010.

[21] C. Henriques, R. Vidinha, D. Botequim, J. P. Borges, and J. A. M. C. Silva, "A systematic study of solution and processing parameters on nanofiber morphology using a new electrospinning apparatus," *Journal of Nanoscience and Nanotechnology*, vol. 9, no. 6, pp. 3535–3545, 2009.

[22] J. Wang, R. Ye, Y. Wei et al., "The effects of electrospun TSF nanofiber diameter and alignment on neuronal differentiation of human embryonic stem cells," *Journal of Biomedical Materials Research A*, vol. 100, no. 3, pp. 632–645, 2012.

[23] Y. Liu, Y. Ji, K. Ghosh, R. A. F. Clark, L. Huang, and M. H. Rafailovich, "Effects of fiber orientation and diameter on the behavior of human dermal fibroblasts on electrospun PMMA scaffolds," *Journal of Biomedical Materials Research A*, vol. 90, no. 4, pp. 1092–1106, 2009.

[24] H. B. Wang, M. E. Mullins, J. M. Cregg, C. W. McCarthy, and R. J. Gilbert, "Varying the diameter of aligned electrospun fibers alters neurite outgrowth and Schwann cell migration," *Acta Biomaterialia*, vol. 6, no. 8, pp. 2970–2978, 2010.

[25] N. Bhattarai, D. Edmondson, O. Veiseh, F. A. Matsen, and M. Zhang, "Electrospun chitosan-based nanofibers and their cellular compatibility," *Biomaterials*, vol. 26, no. 31, pp. 6176–6184, 2005.

[26] C. Vaquette, C. Kahn, C. Frochot et al., "Aligned poly(L-lactic-co-e-caprolactone) electrospun microfibers and knitted structure: a novel composite scaffold for ligament tissue engineering," *Journal of Biomedical Materials Research A*, vol. 94, no. 4, pp. 1270–1282, 2010.

[27] J. P. Kaiser, T. Buerki-Thurnherr, and P. Wick, "Influence of single walled carbon nanotubes at subtoxical concentrations on cell adhesion and other cell parameters of human epithelial cells," *Journal of King Saud University—Science*, vol. 25, no. 1, pp. 15–27, 2013.

[28] J. Kaiser, P. Wick, P. Manser, P. Spohn, and A. Bruinink, "Single walled carbon nanotubes (SWCNT) affect cell physiology and cell architecture," *Journal of Materials Science: Materials in Medicine*, vol. 19, no. 4, pp. 1523–1527, 2008.

[29] K. Nave and J. L. Salzer, "Axonal regulation of myelination by neuregulin 1," *Current Opinion in Neurobiology*, vol. 16, no. 5, pp. 492–500, 2006.

[30] D. D'Urso, P. J. Brophy, S. M. Staugaitis et al., "Protein zero of peripheral nerve myelin: biosynthesis, membrane insertion, and evidence for homotypic interaction," *Neuron*, vol. 4, no. 3, pp. 449–460, 1990.

[31] D. M. Menichella, E. J. Arroyo, R. Awatramani et al., "Protein Zero is necessary for E-cadherin-mediated adherens junction formation in Schwann cells," *Molecular and Cellular Neuroscience*, vol. 18, no. 6, pp. 606–618, 2001.

[32] L. B. Spiryda, "Myelin protein zero and membrane adhesion," *Journal of Neuroscience Research*, vol. 54, no. 2, pp. 137–146, 1998.